IEEE Access
Multidisciplinary | Rapid Review | Open Access Journal

Received 1 March 2024, accepted 13 March 2024, date of publication 22 March 2024, date of current version 11 April 2024.

Digital Object Identifier 10.1109/ACCESS.2024.3380835

RESEARCH ARTICLE

Infinite Limits of Convolutional Neural Network for Urban Electromagnetic Field Exposure Reconstruction

MOHAMMED MALLIK[1], BENJAMIN ALLAERT[1], ESTEBAN EGEA-LOPEZ[2], DAVY P. GAILLOT[3], JOE WIART[4], (Senior Member, IEEE), AND LAURENT CLAVIER[1,3], (Senior Member, IEEE)

[1]IMT Nord Europe, 59650 Lille, France
[2]Department of Information Technologies and Communications, Universidad Politécnica de Cartagena (UPCT), 30202 Cartagena, Spain
[3]CNRS, UMR 8520-IEMN, Université de Lille, 59650 Lille, France
[4]Chaire C2M, LTCI, Télécom Paris, Institut Polytechnique de Paris, 91120 Palaiseau, France

Corresponding author: Mohammed Mallik (mohammed.mallik@imt-nord-europe.fr)

This work was supported in part by the IRCICA, UAR CNRS 3380, Lille; in part by Métropole Européenne de Lille (MEL); in part by MCIN/AEI/10.13039/501100011033 under Grant PID2020-112675RB-C41; and in part by Beyond5G, a project funded by French Government as part of the Economic Recovery Plan, namely "France Relance," and the investments for the future program.

ABSTRACT Electromagnetic field exposure (EMF) has grown to be a critical concern as a consequence of the ongoing installation of fifth-generation cellular networks (5G). The lack of measurements makes it difficult to accurately assess the EMF in a specific urban area, as Spectrum cartography (SC) relies on a set of measurements recorded by spatially distributed sensors for the generation of exposure maps. However, when the spatial sampling rate is limited, significant estimation errors occur. To overcome this issue, the exposure map estimation is addressed as a missing data imputation task. We compute a convolutional neural tangent kernel (CNTK) for an infinitely wide convolutional neural network whose training dynamics can be completely described by a closed-form formula. This CNTK is employed to impute the target matrix and estimate EMF exposure from few sensors sparsely located in an urban environment. Experimental results show that the kernel, even when only sparse sensor data are available, can produce accurate estimates. It is a promising solution for exposure map reconstruction that does not require large training sets. The proposed method is compared with other deep learning approaches and Gaussian Process regression.

INDEX TERMS 5G EMF exposure, kernel regression, neural tangent kernel, infinite width convolutional neural network, semi-supervised learning.

I. INTRODUCTION

Technologies for wireless communication have become a part of our everyday life. Radio-frequency electromagnetic fields (RF-EMFs) are used to enable many modern devices to communicate via cellular networks, Wi-Fi, Bluetooth, and many other technologies. Therefore, the effects of exposure to wireless systems need to be monitored. Even though 5G claims to be more energy efficient than previous generations, there are growing concerns over the deployment of the 5G network for several reasons [1], [2], [3] and in particular higher frequencies, the implementation of ultra-dense base stations and beam-forming.

In Europe, "one-time" measurement programs are frequently conducted for EMF monitoring [3], [4]. Lexnet [5] and other initiatives investigated population radio frequency exposure. Mobile devices and base stations that emit EMFs for radio communication must comply with regulatory levels of human exposure. For instance, several organizations, including the International Commission on Non-Ionizing Radiation Protection (ICNIRP) and the Institute of Electrical and Electronics Engineers (IEEE), have conducted research on human exposure standards [6], [7]. But transmitted signals from base stations and mobile devices generating EMF

The associate editor coordinating the review of this manuscript and approving it for publication was Sandra Costanzo.

exposure are impacted by many factors such as building topology, roads, mobility in road traffic, etc. In addition, it is not possible to track the activity on multiple networks in real time. Thus, reconstructing the EMF exposure map in an urban region is challenging. It could then be of interest to use fixed sensors for monitoring the EMF exposure [8].

This work aims to reconstruct the RF-EMF exposure map of a 1 km^2 rectangular area, discretized into a $M \times N$ grid in Lille city center, France, using only sparsely distributed fixed sensors located in that area and machine learning models. A sensor located at position (m, n) in the grid, where $m \in \{1, \cdots, M\}$ and $n \in \{1, \cdots, N\}$ can measure the exposure locally in that area, i. e. the sensor located at (m, n) can acquire the exposure $e_{(m,n)} \in \mathbb{R}$. If every location (m, n) has a sensor, an exposure map matrix $\gamma \in \mathbb{R}^{M \times N}$ would be constructed. However, placing sensors at every location in the selected area is not a viable option. Hence, the task of exposure map reconstruction is to estimate the complete exposure map γ using the sparsely distributed sensor measurements. One of the major problems is that there are no reference maps covering the entire area. In previous work, a ray-tracing simulator was used to generate the complete reference maps and train the neural networks [9]. These simulations are complex tasks because they involve taking into account a large number of base stations, different technologies and operators, and network configurations that are unknown to us, such as the powers and beams used by the base stations.

Based on a few sparsely distributed sensors, the proposed contribution is to train an infinitely wide Convolutional Neural Network [10], [11] (CNN) for matrix completion/matrix imputation to reconstruct the exposure map. The advantages of wider neural network models for generalization and efficiency in classification and feature learning tasks have been highlighted in numerous recent experiments [12], [13] but have never been applied to EMF reconstruction. Proposed method is based on an innovative approach exploiting the width limits of neural networks. In the infinite width limit [14], [15], [16], [17], artificial neural networks (ANNs) are comparable to Gaussian processes, which relates them to kernel methods. The proposed approach (noted EME-CNTK - Exposure Map Estimation Convolutional Neural Tangent Kernel) takes this concept further by filling in the sparse exposure map using a Convolutional Neural Tangent Kernel (CNTK) [18]. This method is inspired by the imputation of unobserved data into a matrix, also known as image inpainting. The efficiency of the suggested technique is demonstrated by evaluations conducted across a narrow frequency band, 5.89 GHz. It should be noted that the methodology can easily be extended to examine EMF exposure from various technologies, or even combinations, the limitation coming here from the full reference map generation needed for the method evaluation rather than from the reconstruction technique itself. To evaluate and compare the performance of the proposed model, other reconstruction techniques, such as EMGAN [9] and EME-NET [19], are considered. Despite relying on a few fixed sensors only, the developed method performs well in terms of reconstruction.

The main contributions of this paper can be summarized as follows:

- We propose an innovative approach called EME-CNTK, exploiting the width limits of neural networks to faithfully and quickly reconstruct an exposure field. Knowledge of the terrain is injected into the network to guarantee the consistency of the reconstructed data.
- We assess the performance of the proposed approach for reconstructing an exposure field in an urban area using a limited number of sensors. A complementary study of the inference time of the learning model is carried out, highlighting the capacity of the model to perform this task very quickly.

The paper is structured as follows: Section II reviews the main research and progress carried out on the estimation of exposure fields. The scope and background of the study are explained in section III-A. Section III-A describes the proposed EME-CNTK approach for estimating an exposure field in an urban environment from a limited set of sensors. Qualitative and quantitative evaluations highlighting the performance of the proposed approach are conducted in Section IV. The discussion and conclusion are given in Section V and VI.

II. RELATED WORKS

This section presents different strategies that have been used to address the exposure evaluation. We can differentiate four different approaches based on propagation models, stochastic geometry, kriging, or deep learning.

A. DETERMINISTIC AND EMPIRICAL PROPAGATION MODELS

In a given urban region, it is highly complex to evaluate exposure maps with accuracy. Deterministic propagation tools like Veneris-Opal [20] and Atoll [21] are based on Ray Tracing (RT) methods, where the propagating field is simulated with an array of rays that go through the environment and reflect, diffract, and scatter. These techniques use the Maxwell equations' high-frequency approximation (optical ray). They need to simplify the true propagation mechanisms and environmental parameters and are not well adapted to dynamic situations. Despite their significant processing requirements and the fact that their performance depends on the correctness of the tridimensional model of the environment [22], RT and other empirical or semi-empirical propagation models like close-in (CI), floating intercept (FI), alpha, beta or gamma (ABG) [23], [24], [25], are often used to predict power coverage in metropolitan areas (see for instance [26], [27], [28], [29]). But to assess the EMF level, one needs to consider all active networks and devices, which is practically not feasible.

B. STOCHASTIC GEOMETRY APPROACH

The concept of using stochastic geometric in wireless communications is not new [30]. Numerous works have used it, including localization, automobile radar [31], and cumulated interference power [32]. Stochastic geometry is a useful tool to provide the mean exposure or Cumulative Distribution Function (CDF) of exposure [33]. However, this estimated information is not directly related to the spatial location of the user or the specific spot to be studied. Measurements obtained from a drive test are used to parameterize the models [33], [34], [35] and the outcome is a single map representing the mean exposure rather than a dynamic map.

C. KRIGING

The Gaussian process regression, commonly known as kriging [36], is the traditional approach for interpolating geographical data. Kriging has been used in several studies to reconstruct exposure maps [37], [38], [39], [40]. For instance, Solin et al. [41] interpolated magnetic field maps using data on the trajectory of a moving robot in an indoor scenario using a Gaussian process or a kriging approach, assuming so a constant field. However, time evaluation was not considered in any of these studies resulting in one single map of the target area. Furthermore, the current body of scientific literature lacks substantial evidence or comprehensive research regarding the ability to accurately model EMF exposure through the implementation of Gaussian processes. This knowledge gap necessitates further investigation in order to establish a more robust understanding of the relationship between EMF exposure and its potential modeling methodologies. Future studies should aim to fill this gap by conducting rigorous experiments and analyses to verify the effectiveness and limitations of using Gaussian processes to model EMF exposure.

D. NEURAL NETWORK AND MATRIX COMPLETION APPROACH

The standard approaches work effectively for coverage maps, rarely consider the presence of wide and unknown variations in the system such as the change of locations or number of active users. To address this issue, learning-based methods using neural networks are emerging in the field of EMF exposure study. Few studies have used artificial intelligence to forecast the uplink (UL) and downlink (DL) exposure of mobile phones. Specifically, some works have employed machine learning models, specifically artificial neural network (ANN), to predict the power emitted by a mobile phone, which is equivalent to UL exposure [42], [43], as well as to estimate the DL exposure [44], [45]. The models for UL exposure prediction use readily available parameters, such as DL connection indicators (e.g., reference signal received power) and environmental information, as input features. Some approaches are based on measurement data from indoor and outdoor environments to account for realistic scenarios [19], [45]. They employ supervised learning to estimate the levels of EMF exposure in the DL and UL in multi-source indoor WiFi settings. Convolutional neural networks were proposed to reconstruct DL exposure maps in indoor spaces. However, the accuracy of these models was evaluated solely on simulation data, indicating that prior knowledge of measurements or simulations was necessary for effective implementation.

Indeed, learning based methods require labeled data for training. However, it is impossible to measure such reference full maps, so simulated training sets must be used. To avoid this requirement, standard kriging interpolation methods have been used to infer exposure to EMFs and train the models. However, the quality of model reconstruction is strongly linked to the ability of the Kriging method to infer reference maps. Xu et al. [46] have taken into account urban cognitive radio networks and estimated the power spectrum (PS) map using a CNN-based Generative Adversarial Network (GAN). 25 MHz and 75 MHz were used as the bandwidths, and a uniform distribution of users was assumed. A GAN model built based on autoencoder analogy was used to reconstruct images using the under-sampled power spectrum maps as input. To generate full PS maps for training, the authors used the inverse polynomial law model. Zhuo et al. [47] used a self-supervised technique using GAN to generate a full RF map of the selected area from an undersampled RF Map. In that work, to train the model K-nearest neighbor algorithm is used to generate the reference maps. Wang and Wiart [45] estimated exposure in an urban environment from few sensor data using an ANN but full map reconstruction was not considered. Two articles published recently [48], [49] presented deep learning methods for estimating radio maps. A CNN model is used by the authors to estimate the radio map for each Tx-Rx position. However, the network must be trained using a new city map and each trained network specifies a unique map.

Another way to generate the training set is to employ a deterministic radio propagation simulator. Mallik et al. [19] proposed to use the UNet architecture to infer EMF from Wi-Fi access points in an indoor environment. Extensions have been proposed based on conditional GANs [9], where inference is conditioned by physical laws or structural constraints. In both cases, full exposure maps were generated with Ray-Tracing simulators, which raises a major problem: simulated maps are not perfect and require time and expertise to evaluate.

Finally, several works have been done using matrix completion for radio map estimation [50], [51], avoiding the training phase with reference maps and where kernel methods are not used. For example, Wang et al. [52] used matrix completion for low-ranked matrices to construct radio maps in an indoor system.

Our objective is to consider an infinitely wide neural network based approach that does not require a large dataset (full reference maps) to be trained on. This objective can be

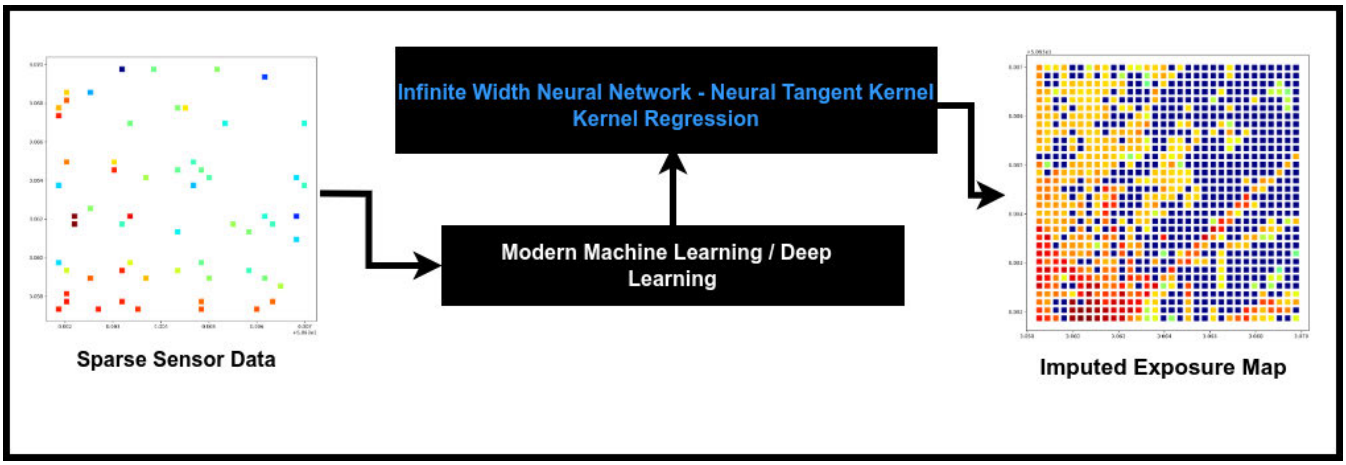

FIGURE 1. Overview of the proposed EME-CNTK approach, which exploits the width limits of neural networks to faithfully and rapidly reconstruct an exposure field. Based on a set of measurements from a sparse sensor network and the terrain map, the neural network, based on ConvNet, infers a coherent exposure field. The main contribution lies in the computation of kernels and the priors.

achieved using the recently proposed Neural Tangent Kernel (NTK) [53] approach.

III. RECONSTRUCTION METHOD

A. SCOPE AND BACKGROUND

Several techniques for imputing missing values using learning-based approaches rely on statistics gathered throughout the entire dataset. They use supervised algorithms that depend on datasets containing complete observations to identify correlations between available data and missing data [54], [55], [56], [57], [58], [59]. Another alternative for imputing missing data is to rely on unsupervised methods. These methods are based on variational autoencoders (VAEs) [60], [61] or generative adversarial networks (GANs) [62], [63]. In [64], a generic framework for missing data imputation on time series is developed by combining concepts from VAEs [65], Cauchy kernels [66], Gaussian Processes [67], structured variational distributions with efficient inference [68] and a particular Evidence Lower Bound (ELBO) for missing data [61]. A new structured variational approximation, the non-linear dimensionality reduction in the presence of missing data, is accomplished using the VAE method. In [69], authors designed variational graph autoencoders for matrix completion to infer air quality from a limited number of measurements. Deep matrix factorization [70] and nuclear norm minimization [71], [72] are examples of common methods for matrix completion to produce low-rank matrices. A low-rank completion is however often inefficient for image inpainting and reconstruction since it ignores local image structure [73], [74]. Several works for image inpainting/reconstruction [74], [75], [76], [77] and supervised and unsupervised infinitely wide neural network [78], [79], [80] for prediction. Authors of [75] introduced an innovative approach for unsupervised 3D shape completion and reconstruction using incomplete scanned data. Their method involves crafting a deep prior based on the NTK concept. Remarkably, the CNN-trained completion of shape patches exhibits a striking resemblance to pre-existing patches. This resemblance arises from their close proximity within the kernel feature space shaped by the NTK. In [81], [82], and [83], it is shown that for any design composed of convolutions, skip-connections, and ReLUs, the network converges nearly certainly to its NTK in the infinite width limit. Works published involving recurrent NTK, residual CNTK, and residual convolutional Gaussian process kernel and others can be found in [84], [85], [86], and [87]. In the research of Arora et al. [18], the derivation and application of CNTK demonstrated enhanced performance for optimization and generalization. Notably, this study provided a non-asymptotic proof, establishing the equivalence between a fully-trained, sufficiently wide neural network and the kernel regression predictor with NTK which can outperform standard CNNs on small data tasks.

In this work, we propose to address the exposure map reconstruction problem as missing data imputation in matrices using infinitely wide CNN for CNTK [18]. The exposure map is reconstructed using only data recorded from a few sparse sensor values in a 1 km^2 area. A high-level overview of the proposed approach is depicted in Figure 1.

B. GENERAL APPROACH

Recently, several works highlighted that training neural networks when the width size approaches infinity is similar to solving kernel regression with the NTK [18] and [88]. Thus, training an unbounded size network is analogous to solving a linear system because the NTK can be quickly calculated in closed form for fully connected networks [53], [89]. The goal is to impute the unseen entries in a matrix $\gamma \in \mathbb{R}^{M\times N}$ given that only a subset of its coordinates has been observed. Examples of the matrix γ are depicted in Figure 2. Both figures show the same exposure field in matrix form but with different measurements depending on the number of sensors 60 (2-B) and 100 (2-A), and also on their location.

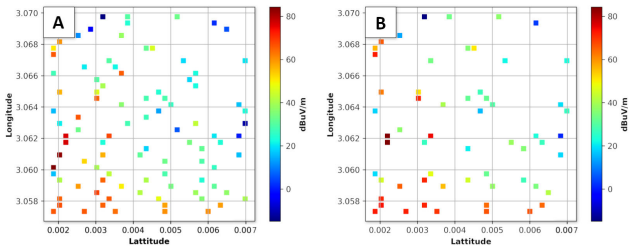

FIGURE 2. Sparse exposure matrix γ with (a) 100 sensors and (b) 60 sensors in $1km^2$ area.

C. METHODOLOGY

In traditional supervised learning, the target is to learn a mapping function between data X and labels Y. The feed-forward deep neural network is a function γ_ψ that can be represented as:

$$\gamma_\psi(x) = \gamma_{\psi_k}\phi(\gamma_{\psi_{k-1}}\phi(\gamma_{\psi_{k-2}}\phi(\ldots(\gamma_{\psi_1}(x))\ldots)), \quad (1)$$

where x is the input and $\gamma_\psi \in \{1, \cdots, k\}$, are the layer functions. Layer functions can be designed as required, but commonly they are formed by connecting simple scalar-valued functions called neurons, which represent a linear function followed by a non-linear function as activation ϕ [90]. Traditionally, convolutional, pooling, and fully connected layers are implemented as layer functions. The vector ψ_k contains the parameters of the neural network, which are updated during the training phase. In [45], exposure in an urban area in Paris city was estimated using an artificial neural network from a few sparsely distributed sensors. In that work, the ANN model was trained by minimizing mean squared error (MSE) loss while having five input features such as location, transmitter distance to sensors, etc. In our method, exposure values from sensors in γ are modeled using a neural network function γ_ψ in (1).

The work by Jacot et al. [53] demonstrates that in the case of over-parameterized or infinitely wide neural networks, their behavior closely mimics that of a kernel function. Consequently, solving kernel regression with NTK, as outlined by [18], [53], is equivalent. The definition of NTK is given by:

Definition (Neural Tangent Kernel) *Let $f(w) : \mathbb{R}^P \to \mathbb{R}$ denote a neural network with initial parameters $w^{(0)}$. The **neural tangent kernel,** $K : \mathbb{R} \times \mathbb{R} \to \mathbb{R}$ is a positive semi-definite function given by:*

$$K(x, x') = \langle \nabla f_x(w^{(0)}), \nabla f_{x'}(w^{(0)}) \rangle, \quad (2)$$

where $w^{(0)} \in \mathbb{R}^P$ denotes the parameters at initialization.

Using Convolutional NTK (CNTK) for exposure map reconstruction is a mapping of element coordinates in the matrix γ to the observed entries present in γ. The CNTK [18] is constructed from a convolutional network with a different number of layers, kernel size, and convolution incorporated with down and upsampling. The link between the CNN model and the CNTK is given by:

$$K(x, x') = \langle \frac{\delta f(\theta, x)}{\delta W_{i,j,k,l}} \times \frac{\delta f(\theta, x')}{\delta W_{i,j,k,l}} \rangle, \quad (3)$$

where x and x' are input samples, θ represents parameters of the network, $\sum_{i,j,k,l}$ denotes the summation over the indices of the convolutional filters and their corresponding weights W,and the L-th layer CNTK kernel is given by:

$$K(x, x') = [\Theta^L(A, A')]_{i,j,i',j'} \quad (4)$$

A is a matrix, it is defined as $A \in \mathbb{R}^{C \times M \times N}$, where C is the number of information channels. In unsupervised neural networks, previous studies have demonstrated that using priors [91], [92], [93] which are drawn from a stationary distribution can perform well [91], [94] for inpainting tasks, even better than only using the corrupted images. In this work, we used a prior to initialize A. The accuracy of the reconstruction is influenced by this prior that captures the relationship among the coordinates within the target matrix, resembling semi-supervised learning and such priors are extensively used in tasks related to image inpainting [91]. We kept two priors giving good results: a sensor-based prior (SBP), where A contains the sensor data at one time stamp or, a random i.i.d. tensor, where the channels are taken from a normal distribution (random normal prior - RNP).

D. MODEL ARCHITECTURE

During training, at initialization, a convolutional neural network is used and the kernel is derived when the Network's width tends to be infinity. We choose a CNN with eight convolutional layers following the architecture used in [91], where each layer is accompanied by *ReLU* or *LeakyReLU* activation. To change The spatial dimensions of the feature maps transposed convolution or nearest neighbor and bilinear interpolation is used and the slope of the activation is set to 0.05 and a stabilization technique is applied to mitigate exploding or vanishing gradient issues during training. Model parameters, layers, and activation functions, training methods are taken from [95] and [96]. The weights and filters are initialized from a Gaussian distribution with mean 0 and std. deviation 1.

The dimension of the matrix can be 32×32, 64×64, 128×128. In this work, the dimension of the grid was limited to 32×32 and 64×64 and only 60 observations from the sparsely distributed sensors are available.

E. RECONSTRUCTING THE MAP

The goal of kernel Regression with CNTK is to fill in missing entries (missing exposure values) as a linear combination of training examples (observed exposure values) in the sparse exposure map image.

The sparse exposure image γ (see Fig. 2) has dimensions $M \times N$ (in the following sections, we will choose $M = N = 32$ or 64). Let $\mathbf{X}$ be the set of measured point locations and $\mathbf{y}$ the corresponding measured values; $\mathbf{x}$ is the location

of an unobserved point where we try to predict the field. As described in [18] the predicted value $\hat{\gamma}(\mathbf{x})$ is given by:

$$\hat{\gamma}(\mathbf{x}) = K(\mathbf{x}, \mathbf{X})^T . K(\mathbf{X}, \mathbf{X})^{-1} . y \tag{5}$$

where $K(\mathbf{x}, \mathbf{X})$ is the CNTK evaluated between the location where the prediction is to be made and the training data X and $K(\mathbf{X}, \mathbf{X})$ is the CNTK evaluated on the training data X.

IV. RESULTS

A. EVALUATION PROTOCOL

1) EVALUATION METRICS

To evaluate the performance of our system, we use two different metrics.

The error $|y - \hat{y}|$ between the predicted value $\hat{y}$ and the reference value y is initially utilized. A comprehensive representation of this error metric is achieved by employing the probability density function (PDF) or cumulative distribution function (CDF). We use a non-parametric kernel density estimation of these functions:

$$f_h(x) = \frac{1}{nh} \sum_{i=1}^{n} K(\frac{x - x_i}{h}), \tag{6}$$

where K is the kernel a non-negative function, $h > 0$ is a smoothing parameter called the bandwidth, n the number of available samples and x_i the sample values. In the following, we use a Gaussian kernel. To have a summarized metric we will consider the root mean squared error (RMSE) [97] given by:

$$RMSE = \sqrt{\frac{1}{n} \sum_{i=1}^{n} \left(Y_i - \hat{Y}_i\right)^2}. \tag{7}$$

The error ratio R and the RMSE tend to emphasize the errors on large values and a relatively small error on a large value can have a larger impact than a relatively large error on a small value. To have a balanced view on this point, we also analyze the error ratio R. We define it as the ratio between the reconstructed map and the reference map, which is given by:

$$R = 10 \log_{10} \left(\frac{\hat{y}}{y}\right). \tag{8}$$

The ratio can then be seen as better emphasizing the error itself. It can also be difficult to interpret because a small error on a very small value can lead to a large error ratio, while the error is in fact not significant. Consequently, when using the error ratio we use a threshold ($0.007\ V/m$), below which we suppress the values. The choice of the threshold suppresses low impacting field values and keeps a sufficiently large number of values to estimate the distribution functions.

2) EVALUATION DATASET

The region of interest (RoI), Lille city center, is an area of 1 km^2. To evaluate the performance of the method, a 1.5-meter height grid is defined as sensor locations, as shown in Figure 3. One or two transmitters are placed in the RoI.

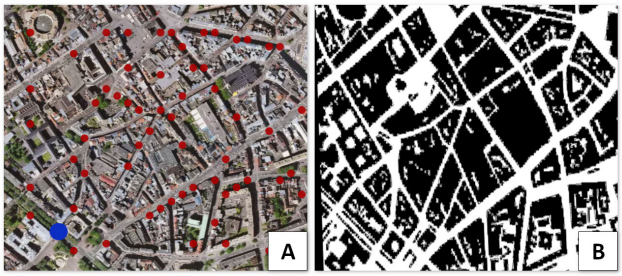

FIGURE 3. The region of interest. a) shows the experimental 1km^2 area, red and blue represent sensor and transmitter respectively, and b) shows the city topology extracted as raster from OpenStreetMap.

The exposure data for the sensors were generated for 20, 40, 60, and 100 sparsely located sensors using Veneris simulator. Different transmitter positions were used to generate different maps. The transmission frequency is 5.89 GHz with 120 W transmitting power. If a full exposure would require a full bandwidth analysis, this choice is necessary for the reference maps simulations. It however does not impact the EME-CNTK methodology which can be extended to a full exposure analysis. Even, the addition of many frequencies and technologies will make the field smoother, making the reconstruction probably slightly easier, and improving its accuracy. Moreover, to implement the city topology effect in the proposed method, the environment (buildings, roads, etc.) has been extracted from OpenStreetMap. The dataset consists of matrices, where each matrix is $\gamma \in \mathbb{R}^{M \times N}$, where M and N are the number of rows and columns of the map grid.

To make the neural networks robust to different changes in factors, e.g., sensor location or measures, the authors generated a different scenario by changing the transmitter location for each map.

3) EME-NET, EMGAN, AND GAUSSIAN PROCESS REGRESSION.

We compare the EME-CNTK with the EME-Net [19] and the EMGAN [9], that have been shown to be effective for this task. These supervised deep learning models are pre-trained on a dataset utilized in [9]. The test data corresponds to a set of 100 matrices, each matrix containing 60 measurements as exposure fields as sensor data defined on the Lille topology illustrated in Figure 3. Both models are trained on 2900 images and tested on 100 images. All dataset were generated using Veneris [20] the 3D ray tracing network simulator.

We have also compared our proposed method with Gaussian Process (GP) regression using the Random Fourier Features (RFF) to obtain the kernel. The GP model was trained on each matrix for 300 epochs with a learning rate of 0.01 and ADAM optimizer.

B. VISUAL ANALYSIS

Figure 4 shows the effectiveness of the proposed approach compared with the generative approaches EME-Net and

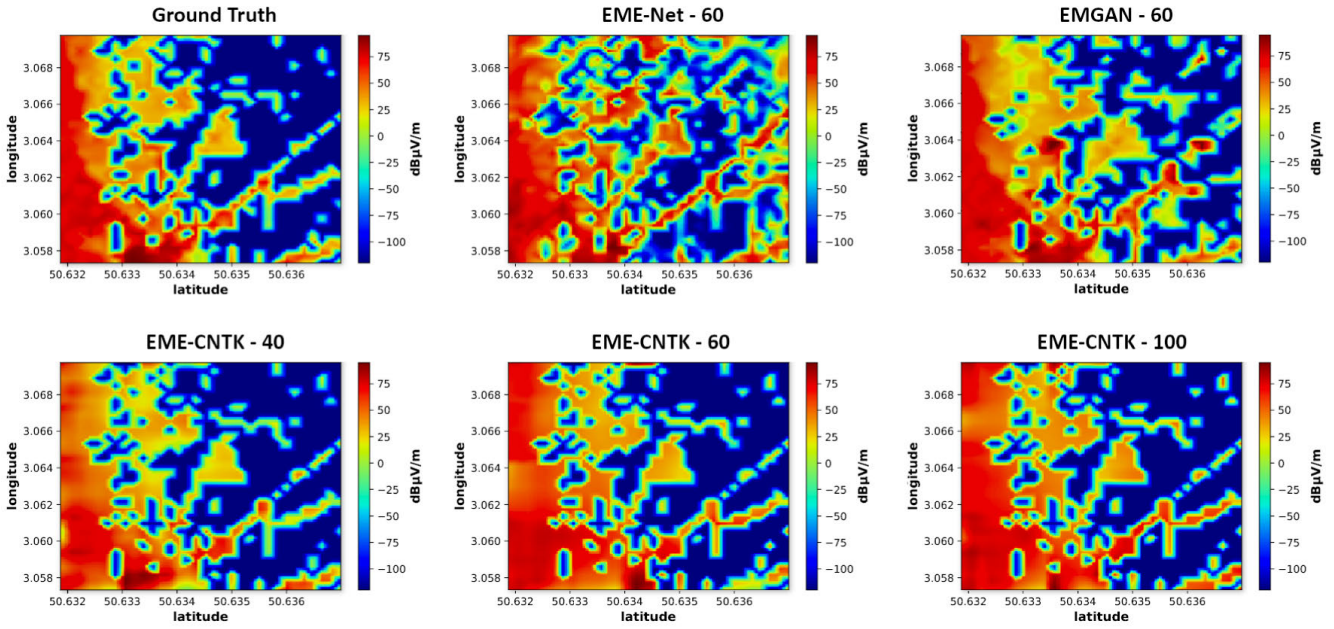

FIGURE 4. Comparison of inferred exposure maps of the proposed method, EME-Net, and EMGAN with reference map simulated by Veneris (reference values).

EMGAN, which looks satisfying even with only 40 measurements as an input.

In Figure 5 (error maps), the estimation errors for all solutions remain reasonably small but in some places, especially at the edge of the image. In these areas, the generative approaches tend to overestimate the EMF, which can be explained by the absence of measurement sensors all around the prediction points but only on one side.

In the presence of a sparse number of sensors, the EMGAN, which takes the street maps (Figure 3-B) as a conditionnal input, reaches better performance, at the price of a very high training cost. EME-Net is less constrained by topology since, the topology image was not used to train the model, and tends to infer exposure fields without real coherence, resulting in a high degree of decorrelation with reference. The EME-CNTK approach performs well without using reference full maps for training compared to generative approaches. This shows the capacity of the approach to well infer the exposure field, without requiring a training phase on the full exposure maps.

Figure 6 shows the comparison between the CNTK map and GP prior with RFF kernel while 60 sensors data was used. The GP has difficulties to correctly account for the city topology and the different propagation properties, depending on the street configurations, while the CNTK better captures the specific topologies.

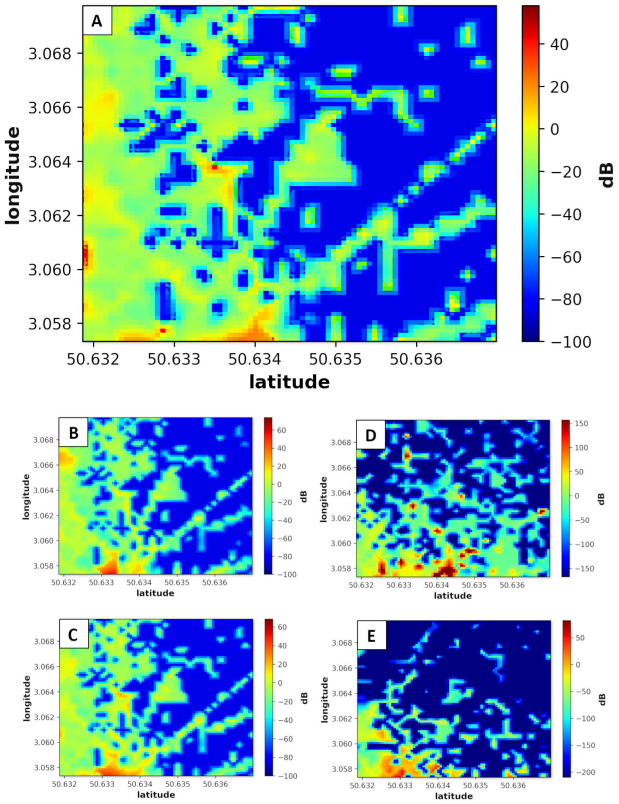

FIGURE 5. Error maps of the proposed method for different numbers of sensors a) EME-CNTK 100 sensors, b) EME-CNTK 60 sensors, c) EME-CNTK 40 sensors, d) EME-Net 60 sensors and e) EMGAN 60 sensors model.

C. QUANTITATIVE ANALYSIS

The PDF of the error ratio (8) and the CDF of the absolute error of the proposed EME-CNTK approach and other models (EME-Net and EMGAN) are shown in Figure 7. In Figure 7-A, we also indicate the mean and variance of the random variable R. We acknowledge that, using 60 sensors, our proposed approach provides superior results

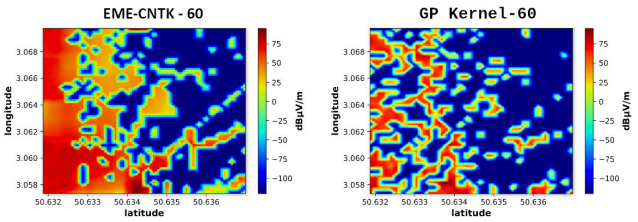

FIGURE 6. Comparison between Reconstructed maps by CNTK - GP prior-RFF kernel.

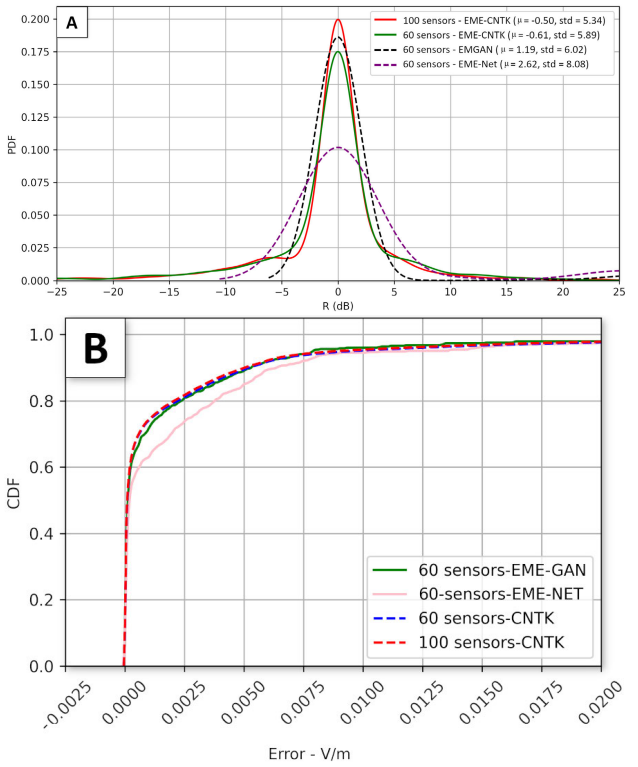

FIGURE 7. EME-CNTK performances and comparison with different models - A) PDF of the ratio R, B) CDF of error. (max. exposure 0.101 V/m.).

than the EME-Net and very close results to the EMGAN. Figure 7-A illustrates significant errors which can be mitigated through the training phase of both EMGAN and EME-Net. However, the proposed approach demonstrate robust performance, while no full reference maps are required in the reconstruction phase, contrarily to EMGAN and EME-Net methods. As evident from our observations, 80% errors are less than $2{,}5.10^{-3}$ V/m when the maximum exposure value was 0.101 V/m in reference values from Veneris. This can be considered as a very low error as an error of $2{,}5.10^{-3}$ V/m is approximately 2.475% relative error of the maximum value of 0.101 V/m.

D. IMPACT OF SENSOR DENSITY.

Figure 4 and 5 illustrates the impact of changing the number of sensors (from 40 to 100). Additionally, Figure 8 shows the EME-CNTK-based reconstructed maps using 40 (Figure 8-B) and 60 sensors (Figure 8-D) measurement points

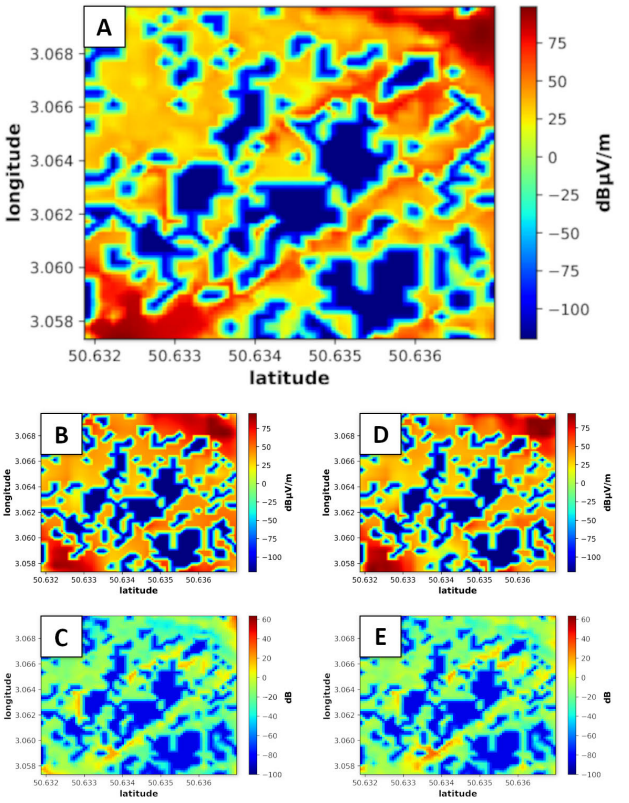

FIGURE 8. Comparison of Reconstructed and error maps of the proposed method when 2 transmitters are used. a) reference map, b) EME-CNTK 40 sensors 2TX, c) EME-CNTK 40 sensors 2TX error map, d) EME-CNTK 60 sensors 2TX, e) EME-CNTK 60 sensors 2TX error map.

when 2 transmitters are in the RoI. Figure 8 illustrates that the performance of the proposed method remains consistent even when 2 transmitters (upper right and bottom left corners) are used. However, in both cases (one or two transmitters), even if the visual inspection is satisfying, some degradation can be observed for 40 sensor-measured maps.

To confirm this comment, Figure 9-A shows the CDF of the error absolute value and Figure 9-B, the probability density function (PDF) of the error ratio R along with the mean and standard deviation of the distribution when different numbers of sensors are used.

When the number of sensors is as low as 20, the mean value is high at 1.39, and the standard deviation is 7.04. When increasing the number of sensors from 40 to 100, the mean value and standard deviation decrease gradually. The standard deviation remains however high due to the large errors that sometimes occur, as seen in the CDF.

Finally, we present in Table 1 the RMSE of the predicted and actual values of exposure. As shown, an increasing number of sensors reduces the RMSE, leading to better reconstruction performance.

The main conclusion is that the density of sensors and how they are distributed play a significant role in the reconstruction process. Further research is needed to optimize the sensors' location and evaluate more carefully the cost of

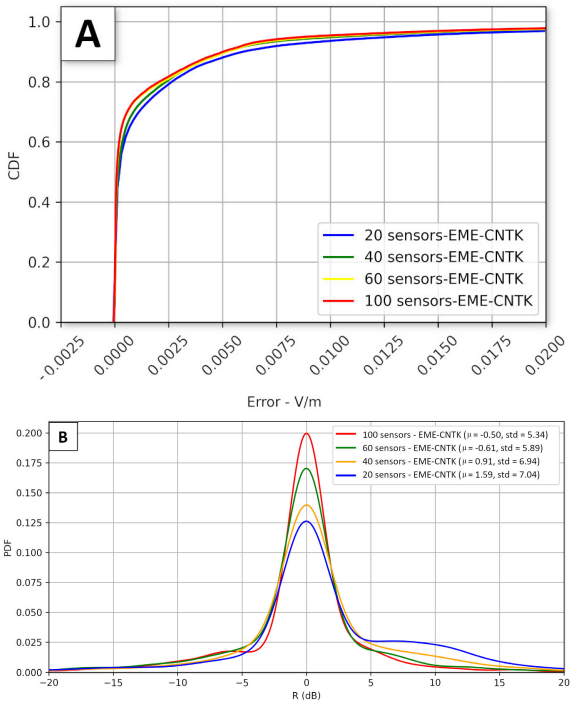

FIGURE 9. EME-CNTK performances - varying number of sensors - A) CDF of error B) PDF of the ratio R (max. exposure 0.101 V/m).

TABLE 1. RMSE of the estimated exposure values using our approach.

Number of sensors	SBP	RNP	GP (RFF Kernel)
20 / km^2	$7{,}47.10^{-3}$	$8{,}43.10^{-2}$	$6{,}93.10^{-3}$
40 / km^2	$6{,}15.10^{-3}$	$1{,}70.10^{-2}$	$6{,}73.10^{-3}$
60 / km^2	$5{,}7.10^{-3}$	$9{,}32.10^{-3}$	$6{,}22.10^{-3}$
100 / km^2	$4{,}35.10^{-3}$	$8{,}12.10^{-3}$	$5{,}64.10^{-3}$

deployment and the accuracy of the maps. To do so, ones needs to take into account the fact that, in a city, the possible locations for sensors are extremely constrained.

E. GRID RESOLUTION

Maintaining uniform sensor density, our objective was to ascertain whether changing in grid resolution influenced prediction accuracy. Figure 10 shows on the left the case of 32×32 maps and on the right the 64×64 case. As expected, the quality of the reconstruction is very similar in both cases, the main difference being the resolution. The proposed EME-CNTK approach adapts perfectly from one resolution to another without applying new training, or specific data augmentation, as required by existing generative approaches such as EME-Net and EMGAN.

To further confirm this result, the CDF of the error absolute value of the reconstructed map compared to the reference exposure map for 64×64 resolution, when EME-CNTK is used, is shown in Figure 11.

When 100 images are analyzed for 11-A is very similar as 10-A, showing no noticeable change in the error between

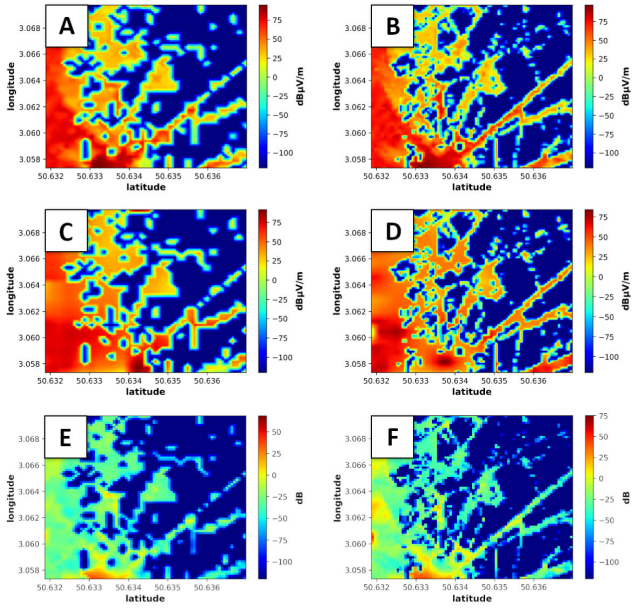

FIGURE 10. Comparison of reconstructed exposure map with reference when different grid size is used. a) Reference map 32×32, b) reference map when resolution is 64×64, c) EME-CNTK - 60 sensors resolution 32×32, d) EME-CNTK - 60 sensors resolution 64×64, e) EME-CNTK - 60 sensors error map resolution 32×32, f) EME-CNTK - 60 sensors error map resolution 64×64.

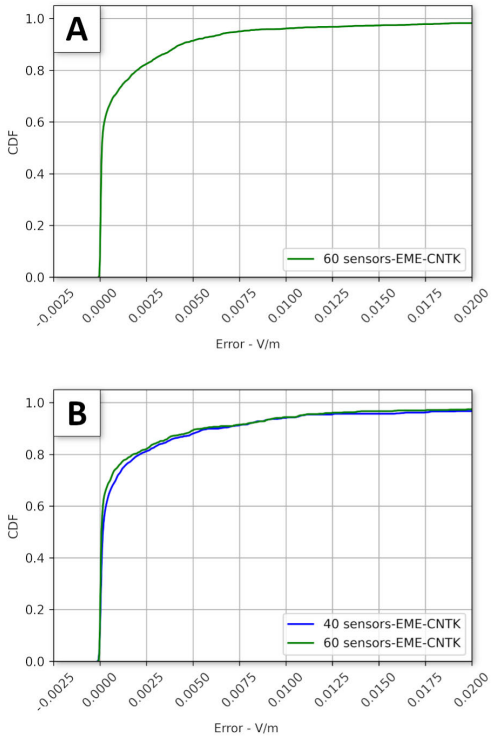

FIGURE 11. a) The CDF of the error (RMSE) between the reconstructed map and reference for 64×64; b) CDF when 2 transmitters are present. 100 images are used to plot the CDF.

32×32 and 64×64 grid sizes. This is rather expected because, while the number of input pixels in comparison to the total number of pixels of the output image is divided by 4,

the density of sensors (per km^2), i.e., the distance between sensors, remains the same.

In 11-B, a similar CDF is plot but the images contain two transmitters. Reconstruction using the proposed EME-CNTK approach is proving effective, yielding approximately 80% error fall under 0.0025 V/m or 2.5mV. This signifies a precision of approximately 2.5% relative to the maximum exposure value 0.101 V/m in the reference values, indicating a high level of accuracy and fidelity in the reconstruction being performed when employing an augmented spatial resolution grid. No difference can be observe in the error when considering one or two transmitters.

F. COMPARATIVE ANALYSIS OF TIME EFFICIENCY

We assessed the efficiency of the proposed method in terms of the time required for inference and training. Our analysis shows that the cGAN-based approach EMGAN and Unet-based approach EME-Net required 1.5 hours and approximately 20 minutes, respectively, to train on a machine with 4GB GPU memory (Intel core i7, NVIDIA Quadro T1000). EMGAN iterated over 139K epochs, while EME-Net trained for 30 epochs. Both models required higher memory, approximately 6-13 GB, and utilized 3.25GB GPU memory for training. In contrast, our proposed EME-CNTK method took only 4,4.10^{-4} seconds to train and impute the matrix as shown in Table 2.

TABLE 2. Comparison of the proposed method with others with machine configuration and time.

Method	Memoryb usage	Weight update/ Training	Inference/ Test
EMEGAN	13GB RAM + 3.2GB VRAM	1.5 Hrs	2s
EME-Net	6GB RAM + 2.5GB VRAM	20 min	1.5s
EME-CNTK	200MB RAM	3,4.10^{-4}s	3,5.10^{-5} s
EME-CNTK	300MB RAM 300MB VRAM	4,1.10^{-4} s	1,1.10^{-4} s

V. DISCUSSION

In this study, we introduced an infinite-width neural network-based approach, EME-CNTK, for estimating EMF exposure in missing points of an area. The proposed method was evaluated and compared with existing techniques, including a cGAN-based approach (EMGAN) and a Unet-based one (EME-Net), across various parameters such as sensor density, grid resolution, and computational efficiency.

Our results showcase the superiority of the EME-CNTK approach over EME-Net and its competitive performance relative to EMGAN. Even utilizing fewer sensors, EME-CNTK consistently outperformed EME-Net and closely approached the accuracy achieved by EMGAN. This observation underscores the effectiveness of our proposed methodology in accurately estimating EMF exposure without the need for full reference maps and time consuming learning, a feature distinct from both other schemes.

One notable advantage of the EME-CNTK approach is its adaptability across varying sensor densities (20 to 100 per km^2) and grid resolutions (32×32 to 64×64). Our analyses revealed that the method maintains consistent performance even with limited sensor deployment and varying grid sizes, showcasing its robustness in real-world scenarios. Furthermore, the EME-CNTK method demonstrated efficiency, requiring significantly less training time (4,1.10^{-4}s) and computational resources compared to cGAN-based EMGAN and Unet-based EME-Net, owing to the simple closed form formula of the tangent kernel [18], [53]. The main advantage of our method is in solving kernel regression with CNTK as it involves solving linear systems of equations, which efficiently handles complex data patterns while optimizing computational resources.

However, it is essential to acknowledge some limitations of our approach. While EME-CNTK yields satisfactory results across different conditions, degradation in performance can be observed with a low density of sensors. Moreover, several neural network designing techniques such as kernel initializers, skip connections, batch normalization, etc. can be utilized in our model to improve the estimation accuracy of the proposed method. Comparing our method with EMGAN, in scenarios involving a sparse number of sensors, EMGAN, which takes street maps (Figure 3-B) as a conditional input, achieves slightly superior performance than our proposed method. Additionally, while the method's adaptability to different grid resolutions was demonstrated, some minor differences in error metrics were observed between resolutions. They remain however negligible for our practical application.

VI. CONCLUSION

We have presented an EMF exposure reconstruction method using CNTK. Compared to other exposure reconstruction techniques, this approach significantly reduces the burden in terms of computational resources (machine configuration, memory, etc.) and time. Moreover, it does not require a large dataset of any reference maps generated from a simulator, which cannot replicate true exposure maps in a realistic network configuration in an urban area, taking into account all the influencing parameters such as base stations from different technologies, the transmitting powers, the beam pattern for 5G, vehicles, houses, trees, etc. When training a generative model, it can take a significant amount of time to reach convergence to optimize the weights, because generative models typically have a large number of parameters and complex architectures. However, from only 60 sparsely located sensor measurements in a 1 km^2 area, the proposed CNTK based method can reconstruct exposure maps rapidly and accurately. In conclusion, the EME-CNTK approach presents a promising solution for EMF exposure estimation, offering a balance between accuracy, efficiency, and adaptability. By leveraging neural network techniques,

our method achieves commendable results even in scenarios with limited sensor deployment and varying grid resolutions. Moving forward, further refinements and validations will be conducted to enhance the method's robustness and applicability in diverse real-world settings.

Future work will concentrate on expanding the estimation of exposure maps using EME-CNTK with the propagation model implemented and in the temporal dimension, with a particular focus on interpreting the CNTK behavior and analyzing the kernel, as suggested in [98].

ACKNOWLEDGMENT

The authors acknowledge the fruitful discussions in the COST Action CA20120 INTERACT.

REFERENCES

[1] A. M. Niknejad, S. Thyagarajan, E. Alon, Y. Wang, and C. Hull, "A circuit designer's guide to 5G mm-wave," in *Proc. IEEE Custom Integr. Circuits Conf. (CICC)*, Sep. 2015, pp. 1–8.

[2] P. Ahokangas, M. Matinmikko-Blue, S. Yrjölä, and H. Hämmäinen, "Platform configurations for local and private 5G networks in complex industrial multi-stakeholder ecosystems," *Telecommun. Policy*, vol. 45, no. 5, Jun. 2021, Art. no. 102128.

[3] P. Gajšek, P. Ravazzani, J. Wiart, J. Grellier, T. Samaras, and G. Thuróczy, "Electromagnetic field exposure assessment in Europe radiofrequency fields (10 MHz–6 GHz)," *J. Exposure Sci. Environ. Epidemiology*, vol. 25, no. 1, pp. 37–44, Jan. 2015.

[4] ANFR. (2017). *Etude De L'exposition Du Public Aux Ondes Radioélectriques*. [Online]. Available: https://www.anfr.fr/fileadmin/mediatheque/documents/expace/20180919-Analyse-mesures-2017.pdf

[5] M. Tesanovic, E. Conil, A. De Domenico, R. Aguero, F. Freudenstein, L. M. Correia, S. Bories, L. Martens, P. M. Wiedemann, and J. Wiart, "The LEXNET project: Wireless networks and EMF: Paving the way for low-EMF networks of the future," *IEEE Veh. Technol. Mag.*, vol. 9, no. 2, pp. 20–28, Jun. 2014.

[6] G. Ziegelberger, R. Croft, M. Feychting, A. C. Green, A. Hirata, G. d'Inzeo, K. Jokela, S. Loughran, C. Marino, S. Miller, G. Oftedal, T. Okuno, E. van Rongen, M. Röösli, Z. Sienkiewicz, J. E. H. Tattersall, and S. Watanabe, "Guidelines for limiting exposure to electromagnetic fields (100 kHz to 300 GHz)," *Health Phys.*, vol. 118, no. 5, pp. 483–524, 2020.

[7] W. H. Bailey, R. Bodemann, J. Bushberg, C.-K. Chou, R. Cleveland, A. Faraone, K. R. Foster, K. E. Gettman, K. Graf, and T. Harrington, "Synopsis of IEEE std c95.1Ů-2019 'IEEE standard for safety levels with respect to human exposure to electric, magnetic, and electromagnetic fields, 0 Hz to 300 GHz," *IEEE Access*, vol. 7, pp. 171346–171356, 2019.

[8] L. Diez, R. Agüero, and L. Muñoz, "Electromagnetic field assessment as a smart city service: The SmartSantander use-case," *Sensors*, vol. 17, no. 6, p. 1250, May 2017.

[9] M. Mallik, A. A. Tesfay, B. Allaert, R. Kassi, E. Egea-Lopez, J.-M. Molina-Garcia-Pardo, J. Wiart, D. P. Gaillot, and L. Clavier, "Towards outdoor electromagnetic field exposure mapping generation using conditional GANs," *Sensors*, vol. 22, no. 24, p. 9643, Dec. 2022.

[10] C. K. I. Williams, "Computation with infinite neural networks," *Neural Comput.*, vol. 10, no. 5, pp. 1203–1216, Jul. 1998.

[11] C. Williams, "Computing with infinite networks," in *Proc. Adv. Neural Inf. Process. Syst.*, vol. 9, 1996, pp. 1–7.

[12] J. Lee, L. Xiao, S. Schoenholz, Y. Bahri, R. Novak, J. Sohl-Dickstein, and J. Pennington, "Wide neural networks of any depth evolve as linear models under gradient descent," in *Proc. Adv. Neural Inf. Process. Syst.*, vol. 32, 2019, pp. 1–12.

[13] V. Nagarajan and J. Z. Kolter, "Uniform convergence may be unable to explain generalization in deep learning," in *Proc. Adv. Neural Inf. Process. Syst.*, vol. 32, 2019, pp. 1–12.

[14] J. Lee, Y. Bahri, R. Novak, S. S. Schoenholz, J. Pennington, and J. Sohl-Dickstein, "Deep neural networks as Gaussian processes," 2017, *arXiv:1711.00165*.

[15] R. M. Neal, *Bayesian Learning for Neural Networks*, vol. 118. Berlin, Germany: Springer, 2012.

[16] G. Pleiss and J. P. Cunningham, "The limitations of large width in neural networks: A deep Gaussian process perspective," 2021, *arXiv:2106.06529*.

[17] A. G. de G. Matthews, M. Rowland, J. Hron, R. E. Turner, and Z. Ghahramani, "Gaussian process behaviour in wide deep neural networks," 2018, *arXiv:1804.11271*.

[18] S. Arora, S. S. Du, W. Hu, Z. Li, R. R. Salakhutdinov, and R. Wang, "On exact computation with an infinitely wide neural net," in *Proc. Adv. Neural Inf. Process. Syst.*, vol. 32, 2019, pp. 1–10.

[19] M. Mallik, S. Kharbech, T. Mazloum, S. Wang, J. Wiart, D. P. Gaillot, and L. Clavier, "EME-net: A U-net-based indoor EMF exposure map reconstruction method," in *Proc. 16th Eur. Conf. Antennas Propag. (EuCAP)*, Mar. 2022, pp. 1–5.

[20] E. Egea-Lopez, F. Losilla, J. Pascual-Garcia, and J. M. Molina-Garcia-Pardo, "Vehicular networks simulation with realistic physics," *IEEE Access*, vol. 7, pp. 44021–44036, 2019.

[21] A. Forsk, "Radio planning & optimisation software," Tech. Reference Guide, Blagnac-France, Copyright by Forsk, 2011.

[22] Z. Yun and M. F. Iskander, "Ray tracing for radio propagation modeling: Principles and applications," *IEEE Access*, vol. 3, pp. 1089–1100, 2015.

[23] G. R. MacCartney, J. Zhang, S. Nie, and T. S. Rappaport, "Path loss models for 5G millimeter wave propagation channels in urban microcells," in *Proc. IEEE Global Commun. Conf. (GLOBECOM)*, Dec. 2013, pp. 3948–3953.

[24] S. Piersanti, L. A. Annoni, and D. Cassioli, "Millimeter waves channel measurements and path loss models," in *Proc. IEEE Int. Conf. Commun. (ICC)*, Jun. 2012, pp. 4552–4556.

[25] J. B. Andersen, T. S. Rappaport, and S. Yoshida, "Propagation measurements and models for wireless communications channels," *IEEE Commun. Mag.*, vol. 33, no. 1, pp. 42–49, 1995.

[26] K. Rizk, J.-F. Wagen, and F. Gardiol, "Two-dimensional ray-tracing modeling for propagation prediction in microcellular environments," *IEEE Trans. Veh. Technol.*, vol. 46, no. 2, pp. 508–518, May 1997.

[27] R. Wahl, G. Wölfle, P. Wertz, P. Wildbolz, and F. Landstorfer, "Dominant path prediction model for urban scenarios," in *Proc. 14th IST Mobile Wireless Commun. Summit, Dresden (Germany)*, 2005, pp. 1–5.

[28] C. A. Balanis, *Advanced Engineering Electromagnetics*. Hoboken, NJ, USA: Wiley, 2012.

[29] T. Zugno, M. Drago, M. Giordani, M. Polese, and M. Zorzi, "Toward standardization of millimeter-wave vehicle-to-vehicle networks: Open challenges and performance evaluation," *IEEE Commun. Mag.*, vol. 58, no. 9, pp. 79–85, Sep. 2020.

[30] F. Baccelli, "Stochastic geometry and wireless networks: Volume II applications," *Found. Trends® Netw.*, vol. 4, nos. 1–2, pp. 1–312, 2009.

[31] C. E. O'Lone, H. S. Dhillon, and R. M. Buehrer, "A statistical characterization of localization performance in wireless networks," *IEEE Trans. Wireless Commun.*, vol. 17, no. 9, pp. 5841–5856, Sep. 2018.

[32] R. Mathar and J. Mattfeldt, "On the distribution of cumulated interference power in Rayleigh fading channels," *Wireless Netw.*, vol. 1, no. 1, pp. 31–36, Mar. 1995.

[33] Q. Gontier, L. Petrillo, F. Rottenberg, F. Horlin, J. Wiart, C. Oestges, and P. De Doncker, "Semi-empirical model of global exposure using stochastic geometry," in *Proc. IEEE Int. Conf. Commun. Workshops (ICC Workshops)*, Jun. 2021, pp. 1–5.

[34] Q. Gontier, L. Petrillo, F. Rottenberg, F. Horlin, J. Wiart, C. Oestges, and P. De Doncker, "A stochastic geometry approach to EMF exposure modeling," *IEEE Access*, vol. 9, pp. 91777–91787, 2021.

[35] C. Wiame, S. Demey, L. Vandendorpe, P. De Doncker, and C. Oestges, "Joint data rate and EMF exposure analysis in Manhattan environments: Stochastic geometry and ray tracing approaches," *IEEE Trans. Veh. Technol.*, vol. 73, no. 1, pp. 894–908, Jan. 2024.

[36] D. G. Krige, "A statistical approach to some basic mine valuation problems on the Witwatersrand," *J. Southern Afr. Inst. Mining Metall.*, vol. 52, no. 6, pp. 119–139, 1951.

[37] S. Aerts, D. Deschrijver, L. Verloock, T. Dhaene, L. Martens, and W. Joseph, "Assessment of outdoor radiofrequency electromagnetic field exposure through hotspot localization using kriging-based sequential sampling," *Environ. Res.*, vol. 126, pp. 184–191, Oct. 2013.

[38] S. Aerts, Y. Huang, L. Martens, W. Joseph, and J. Wiart, "Use of artificial intelligence to model exposure to radiofrequency electromagnetic fields based on sensor network measurements," in *Proc. 4th Workshop Uncertainty Model. Eng. Appl. (UMEMA)*, 2018, pp. 1–2.

[39] A. Martínez-González, J. Monzó-Cabrera, A. J. Martínez-Sáez, and A. J. Lozano-Guerrero, "Minimization of measuring points for the electric field exposure map generation in indoor environments by means of Kriging interpolation and selective sampling," *Environ. Res.*, vol. 212, Sep. 2022, Art. no. 113577.

[40] J. Shan, W. Shao, H. Xue, Y. Xu, and D. Mao, "The method of electromagnetic environment map construction based on Kriging spatial interpolation," in *Proc. Int. Conf. Inf. Syst. Comput. Aided Educ. (ICISCAE)*, Jul. 2018, pp. 212–217.

[41] A. Solin, M. Kok, N. Wahlström, T. B. Schön, and S. Särkkä, "Modeling and interpolation of the ambient magnetic field by Gaussian processes," *IEEE Trans. Robot.*, vol. 34, no. 4, pp. 1112–1127, Aug. 2018.

[42] T. Mazloum, S. Wang, M. Hamdi, B. Ashenafi Mulugeta, and J. Wiart, "Artificial neural network-based uplink power prediction from multi-floor indoor measurement campaigns in 4G networks," *Frontiers Public Health*, vol. 9, Nov. 2021, Art. no. 777798.

[43] R. Falkenberg, B. Sliwa, N. Piatkowski, and C. Wietfeld, "Machine learning based uplink transmission power prediction for LTE and upcoming 5G networks using passive downlink indicators," in *Proc. IEEE 88th Veh. Technol. Conf. (VTC-Fall)*, Aug. 2018, pp. 1–7.

[44] G. Tognola, D. Plets, E. Chiaramello, S. Gallucci, M. Bonato, S. Fiocchi, M. Parazzini, L. Martens, W. Joseph, and P. Ravazzani, "Use of machine learning for the estimation of down- and up-link field exposure in multi-source indoor WiFi scenarios," *Bioelectromagnetics*, vol. 42, no. 7, pp. 550–561, Oct. 2021.

[45] S. Wang and J. Wiart, "Sensor-aided EMF exposure assessments in an urban environment using artificial neural networks," *Int. J. Environ. Res. Public Health*, vol. 17, no. 9, p. 3052, Apr. 2020.

[46] X. Han, L. Xue, F. Shao, and Y. Xu, "A power spectrum maps estimation algorithm based on generative adversarial networks for underlay cognitive radio networks," *Sensors*, vol. 20, no. 1, p. 311, Jan. 2020.

[47] Z. Li, J. Cao, H. Wang, and M. Zhao, "Sparsely self-supervised generative adversarial nets for radio frequency estimation," *IEEE J. Sel. Areas Commun.*, vol. 37, no. 11, pp. 2428–2442, Nov. 2019.

[48] K. Saito, Y. Jin, C. Kang, J.-I. Takada, and J.-S. Leu, "Two-step path loss prediction by artificial neural network for wireless service area planning," *IEICE Commun. Exp.*, vol. 8, no. 12, pp. 611–616, 2019.

[49] T. Imai, K. Kitao, and M. Inomata, "Radio propagation prediction model using convolutional neural networks by deep learning," in *Proc. 13th Eur. Conf. Antennas Propag. (EuCAP)*, Mar. 2019, pp. 1–5.

[50] S. Chouvardas, S. Valentin, M. Draief, and M. Leconte, "A method to reconstruct coverage loss maps based on matrix completion and adaptive sampling," in *Proc. IEEE Int. Conf. Acoust., Speech Signal Process. (ICASSP)*, Mar. 2016, pp. 6390–6394.

[51] M. Tang, G. Ding, Q. Wu, Z. Xue, and T. A. Tsiftsis, "A joint tensor completion and prediction scheme for multi-dimensional spectrum map construction," *IEEE Access*, vol. 4, pp. 8044–8052, 2016.

[52] Z. Wang, L. Zhang, Q. Kong, and K. Wang, "Fast construction of the radio map based on the improved low-rank matrix completion and recovery method for an indoor positioning system," *J. Sensors*, vol. 2021, pp. 1–12, Oct. 2021.

[53] A. Jacot, F. Gabriel, and C. Hongler, "Neural tangent kernel: Convergence and generalization in neural networks," in *Proc. Adv. Neural Inf. Process. Syst.*, vol. 31, 2018, pp. 1–10.

[54] M. Bertalmio, G. Sapiro, V. Caselles, and C. Ballester, "Image inpainting," in *Proc. 27th Annu. Conf. Comput. Graph. Interact. Techn.* New York, NY, USA: ACM Press, 2000, pp. 417–424.

[55] C. Dong, C. C. Loy, K. He, and X. Tang, "Image super-resolution using deep convolutional networks," *IEEE Trans. Pattern Anal. Mach. Intell.*, vol. 38, no. 2, pp. 295–307, Feb. 2016.

[56] W. Freeman, T. Jones, and E. Pasztor, "Example-based super-resolution," *IEEE Comput. Graph. Appl.*, vol. 22, no. 2, pp. 56–65, Apr. 2002.

[57] J. Kim, J. K. Lee, and K. M. Lee, "Accurate image super-resolution using very deep convolutional networks," 2015, *arXiv:1511.04587*.

[58] J. Xie, L. Xu, and E. Chen, "Image denoising and inpainting with deep neural networks," in *Advances in Neural Information Processing Systems*, vol. 25, F. Pereira, C. Burges, L. Bottou, and K. Weinberger, Eds. Red Hook, NY, USA: Curran Associates, 2012.

[59] R. A. Yeh, C. Chen, T. Lim, M. Hasegawa-Johnson, and M. N. Do, "Semantic image inpainting with perceptual and contextual losses," 2016, *arXiv:1607.07539*.

[60] S. K. Ainsworth, N. J. Foti, and E. B. Fox, "Disentangled VAE representations for multi-aspect and missing data," 2018, *arXiv:1806.09060*.

[61] A. Nazábal, P. M. Olmos, Z. Ghahramani, and I. Valera, "Handling incomplete heterogeneous data using VAEs," *Pattern Recognit.*, vol. 107, Nov. 2020, Art. no. 107501.

[62] S. Cheng-Xian Li, B. Jiang, and B. Marlin, "MisGAN: Learning from incomplete data with generative adversarial networks," 2019, *arXiv:1902.09599*.

[63] J. Yoon, J. Jordon, and M. Schaar, "Gain: Missing data imputation using generative adversarial nets," in *Proc. Int. Conf. Mach. Learn.*, 2018, pp. 5689–5698.

[64] V. Fortuin, D. Baranchuk, G. Ratsch, and S. Mandt, "GP-VAE: Deep probabilistic time series imputation," in *Proc. Int. Conf. Artif. Intell. Statist.*, 2020, pp. 1651–1661.

[65] P. K. Diederik and M. Welling, "Auto-encoding variational Bayes," in *Proc. Int. Conf. Learn. Represent. (ICLR)*, vol. 1, 2014, pp. 1–12.

[66] P. Jähnichen, F. Wenzel, M. Kloft, and S. Mandt, "Scalable generalized dynamic topic models," in *Proc. Int. Conf. Artif. Intell. Statist.*, 2018, pp. 1427–1435.

[67] C. E. Rasmussen and C. K. Williams, *Gaussian Processes for Machine Learning*, vol. 1. Cambridge, MA, USA: MIT Press, 2006.

[68] R. Bamler and S. Mandt, "Structured black box variational inference for latent time series models," 2017, *arXiv:1707.01069*.

[69] T. H. Do, D. M. Nguyen, E. Tsiligianni, A. L. Aguirre, V. P. L. Manna, F. Pasveer, W. Philips, and N. Deligiannis, "Matrix completion with variational graph autoencoders: Application in hyperlocal air quality inference," in *Proc. IEEE Int. Conf. Acoust., Speech Signal Process. (ICASSP)*, May 2019, pp. 7535–7539.

[70] S. Arora, N. Cohen, W. Hu, and Y. Luo, "Implicit regularization in deep matrix factorization," in *Proc. Adv. Neural Inf. Process. Syst.*, vol. 32, 2019, pp. 1–12.

[71] B. Recht, M. Fazel, and P. A. Parrilo, "Guaranteed minimum-rank solutions of linear matrix equations via nuclear norm minimization," *SIAM Rev.*, vol. 52, no. 3, pp. 471–501, Jan. 2010.

[72] E. J. Candes and T. Tao, "The power of convex relaxation: Near-optimal matrix completion," *IEEE Trans. Inf. Theory*, vol. 56, no. 5, pp. 2053–2080, May 2010.

[73] Z. Li, Z. J. Xu, T. Luo, and H. Wang, "A regularised deep matrix factorised model of matrix completion for image restoration," *IET Image Process.*, vol. 16, no. 12, pp. 3212–3224, Oct. 2022.

[74] Z. Jia, M. K. Ng, and G. Song, "Robust quaternion matrix completion with applications to image inpainting," *Numer. Linear Algebra Appl.*, vol. 26, no. 4, p. e2245, Aug. 2019.

[75] L. Chu, H. Pan, and W. Wang, "Unsupervised shape completion via deep prior in the neural tangent kernel perspective," *ACM Trans. Graph.*, vol. 40, no. 3, pp. 1–17, Jun. 2021.

[76] A. Radhakrishnan, G. Stefanakis, M. Belkin, and C. Uhler, "Simple, fast, and flexible framework for matrix completion with infinite width neural networks," 2021, *arXiv:2108.00131*.

[77] R. Novak, L. Xiao, J. Hron, J. Lee, A. A. Alemi, J. Sohl-Dickstein, and S. S. Schoenholz, "Neural tangents: Fast and easy infinite neural networks in Python," in *Proc. Int. Conf. Learn. Represent.*, 2020, pp. 1–19.

[78] Z. Li, R. Wang, D. Yu, S. S. Du, W. Hu, R. Salakhutdinov, and S. Arora, "Enhanced convolutional neural tangent kernels," 2019, *arXiv:1911.00809*.

[79] G. Yang and E. J. Hu, "Feature learning in infinite-width neural networks," 2022, *arXiv:2011.14522*.

[80] R. Novak, J. Sohl-Dickstein, and S. S. Schoenholz, "Fast finite width neural tangent kernel," in *Proc. Int. Conf. Mach. Learn.*, 2022, pp. 1–10.

[81] G. Yang, "Tensor programs II: Neural tangent kernel for any architecture," 2020, *arXiv:2006.14548*.

[82] G. Yang and E. Littwin, "Tensor programs IIB: Architectural universality of neural tangent kernel training dynamics," in *Proc. Int. Conf. Mach. Learn.*, 2021, pp. 11762–11772.

[83] B. Adlam, J. Lee, L. Xiao, J. Pennington, and J. Snoek, "Exploring the uncertainty properties of neural networks' implicit priors in the infinite-width limit," 2020, *arXiv:2010.07355*.

[84] D. Barzilai, A. Geifman, M. Galun, and R. Basri, "A kernel perspective of skip connections in convolutional networks," 2022, *arXiv:2211.14810*.

[85] S. Alemohammad, Z. Wang, R. Balestriero, and R. Baraniuk, "The recurrent neural tangent kernel," 2020, *arXiv:2006.10246*.

[86] J. Bradbury et al., "JAX: Composable transformations of Python+NumPy programs," GitHub, 2018. [Online]. Available: http://github.com/google/jax

[87] D. Bracale, S. Favaro, S. Fortini, and S. Peluchetti, "Infinite-channel deep stable convolutional neural networks," 2021, *arXiv:2102.03739*.
[88] A. Bietti and J. Mairal, "On the inductive bias of neural tangent kernels," in *Proc. Adv. Neural Inf. Process. Syst.*, vol. 32, 2019, pp. 1–12.
[89] C. Liu, L. Zhu, and M. Belkin, "On the linearity of large non-linear models: When and why the tangent kernel is constant," in *Proc. 34th Conf. Neural Inf. Process. Syst.*, 2021, pp. 1–11.
[90] J. Heaton, "Ian goodfellow, Yoshua bengio, and Aaron courville: Deep learning: The MIT Press, 2016, 800, pp ISBN: 0262035618," *Genetic Program. Evolvable Mach.*, vol. 19, nos. 1–2, pp. 305–307, Jun. 2018.
[91] V. Lempitsky, A. Vedaldi, and D. Ulyanov, "Deep image prior," in *Proc. IEEE/CVF Conf. Comput. Vis. Pattern Recognit.*, Jun. 2018, pp. 9446–9454.
[92] A. V. Dalca, G. Balakrishnan, J. Guttag, and M. R. Sabuncu, "Unsupervised learning of probabilistic diffeomorphic registration for images and surfaces," *Med. Image Anal.*, vol. 57, pp. 226–236, Oct. 2019.
[93] F. P. Casale, A. Dalca, L. Saglietti, J. Listgarten, and N. Fusi, "Gaussian process prior variational autoencoders," in *Proc. Adv. Neural Inf. Process. Syst.*, vol. 31, 2018, pp. 1–12.
[94] Z. Cheng, M. Gadelha, S. Maji, and D. Sheldon, "A Bayesian perspective on the deep image prior," in *Proc. IEEE/CVF Conf. Comput. Vis. Pattern Recognit. (CVPR)*, Jun. 2019, pp. 5438–5446.
[95] M. Abadi et al., "Tensorflow: A system for large-scale machine learning," in *Proc. OSDI*, vol. 16, 2016, pp. 265–283.
[96] P. Virtanen et al., "SciPy 1.0: Fundamental algorithms for scientific computing in Python," *Nature Methods*, vol. 17, pp. 261–272, Feb. 2020.
[97] T. O. Hodson, "Root-mean-square error (RMSE) or mean absolute error (MAE): When to use them or not," *Geoscientific Model Develop.*, vol. 15, no. 14, pp. 5481–5487, Jul. 2022.
[98] Y. Yu and M. Yao, "When convolutional neural networks meet laser-induced breakdown spectroscopy: End-to-end quantitative analysis modeling of ChemCam spectral data for major elements based on ensemble convolutional neural networks," *Remote Sens.*, vol. 15, no. 13, p. 3422, Jul. 2023.

MOHAMMED MALLIK received the master's degree in electronics and information technology from Germany and the Ph.D. degree from the University of Lille. He is currently a Research Engineer with IMT Nord Europe, a French leading public institute of technology. His research interests include EMF exposure assessment, machine learning, and optimization.

BENJAMIN ALLAERT received the M.S. and Ph.D. degrees in computer science from the University of Lille, France. In 2021, he integrated with IMT Nord Europe, a French leading institute of technology, as an Associate Professor. His research interests include the development of digital simulation, deep learning, and decision models to help humans better interact with their environment.

ESTEBAN EGEA-LOPEZ received the bachelor's degree in telecommunications engineering from Universidad Politècnica de València (UPV), Spain, in 2000, the master's degree in electronics from the University of Gävle, Sweden, in 2001, and the Ph.D. degree in telecommunications from Universidad Politècnica de Cartagena (UPCT), in 2006. He is currently an Associate Professor with the Department of Information Technologies and Communications, UPCT. His research interests include vehicular networks and MAC protocols.

DAVY P. GAILLOT was born in Arras, France, in October 1978. He received the B.Sc. degree in mechanical engineering from École Nationale d'Ingénieurs de Metz (ENIM), Metz, France, in 2002, the M.Sc. degree in mechanics, materials, structures, and processes from the University of Metz, Metz, in 2002, and the Ph.D. degree in materials science and engineering from the Department of Materials Science and Engineering, Georgia Institute of Technology, Atlanta, GA, USA, in 2007. Since 2008, he has been an Associate Professor with the Institut d'Electronique, de Microélectronique et de Nanotechnologie/Télécommunications, Interférences et Compatibilité Electromagnétique—IEMN/TELICE Group, University of Lille 1, Villeneuve d'Ascq, France. His research interests include the development of outdoor/indoor radio channel models for localization techniques that are supported by legacy or upcoming millimeter-wave and centimeter-wave wireless network standards. In addition, he focuses on highly diffuse and industrial radio channels for propagation modeling and exposure assessment.

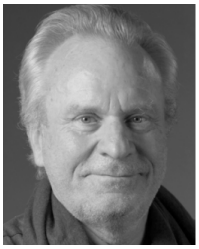

JOE WIART (Senior Member, IEEE) received the Diploma degree in telecommunication engineering, in 1992, the Ph.D. degree, in 1995, and the H.D.R. degree, in 2015. Since 2015, he has been the Holder of the Chair C2M "Caractérisation, Modélisation et Maîtrise of the Institut Mines Telecom," Télécom Paris. His works gave rise to more than 150 publications in journals and more than 200 communications. His research interests include experimental, numerical methods, machine learning, statistics applied in electromagnetism, dosimetry, and exposure monitoring. He has been an Emeritus Member of The Society of Electrical Engineers (SEE), since 2008. He is also the Chairperson of the TC106x of the European Committee for Electrotechnical Standardization (CENELEC) in charge of EMF exposure standards. He is also the past Chairperson of the International Union of Radio Science (URSI) Commission K and has been the Chairperson of the French Chapter of URSI.

LAURENT CLAVIER (Senior Member, IEEE) received the Ph.D. degree in signal processing from TELECOM Bretagne (now IMT Atlantique), Brest, France, and the H.D.R. degree from Lille University, France, in 2009. Since October 2011, he has been a Professor with the Mines-Telecom Institute, IMT Nord Europe. He participated in several European and French-funded projects and has published more than 150 papers and communications. His research interests include digital communications and the physical layer of wireless networks for IoT, more specifically energy autonomous sensor networks, interference models, and impact in ultra-dense wireless networks. He is also the Chair of CA20120 INTERACT "Intelligence-Enabling Radio Communications for Seamless Inclusive Interactions."